

Asymmetric band gap shift in electrically addressed blue phase photonic crystal fibers

M. WAHLE,^{1,2,*} J. EBEL,^{1,2} D. WILKES,³ AND H.-S. KITZEROW,^{1,2}

¹Department of Chemistry, Paderborn University, Warburger Str. 100, 33098 Paderborn, Germany

²Center for Optoelectronics and Photonics (CeOPP), Paderborn University, Warburger Str. 100, 33098 Paderborn, Germany

³Merck KGaA, Division of Performance Materials, BU Liquid Crystal – Research and Development, Frankfurter Str. 250, 64293 Darmstadt, Germany

*markus.wahle@upb.de

<http://go.upb.de/mwahle>

Abstract: In this paper, we present electrooptic experiments on photonic crystal fibers filled with a liquid crystalline blue phase. These fibers guide light via photonic band gaps (PBGs). The blue phase is isotropic in the field-off state but becomes birefringent under an electric field. This leads to a polarization dependent shift of the PBGs. Interestingly, the effect on the PBGs is asymmetrical: while the short wavelength edges of the PBGs shift, the long wavelength edges are almost unaffected. By performing band gap and modal analyses via the finite element simulations, we find that the asymmetric shift is the result of the mixed polarization of the involved photonic bands. Finally, we use the band gap shifts to calculate effective Kerr constants of the blue phase.

© 2016 Optical Society of America

OCIS codes: (160.3710) Liquid crystals; (060.5295) Photonic crystal fibers; (160.5293) Photonic bandgap materials; (230.2090) Electro-optical devices.

References and links

1. S. Meiboom, M. Sammon, and D. W. Berreman, "Lattice symmetry of the cholesteric blue phases," *Phys. Rev. A* **28**(6), 3553–3560 (1983).
2. S. Meiboom, M. Sammon, and W. F. Brinkman, "Lattice of disclinations, The structure of the blue phases of cholesteric liquid crystals," *Phys. Rev. A* **27**(1), 438–454 (1983).
3. H. Choi, H. Higuchi, and H. Kikuchi, "Fast electro-optic switching in liquid crystal blue phase II," *Appl. Phys. Lett.* **98**(13), 7–10 (2011).
4. L. Rao, J. Yan, S. T. Wu, S. I. Yamamoto, and Y. Haseba, "A large Kerr constant polymer-stabilized blue phase liquid crystal," *Appl. Phys. Lett.* **98**(8), 2009–2012 (2011).
5. G. Nordendorf, A. Lorenz, A. Hoischen, J. Schmidtke, H. Kitzerow, D. Wilkes, and M. Wittek, "Hysteresis and memory factor of the Kerr effect in blue phases," *J. Appl. Phys.* **114**(17) (2013).
6. H.-S. Kitzerow, "Blue Phases, Prior Art, Potential Polar Effects, Challenges," *Ferroelectrics* **395**(1), 66–85 (2010).
7. P. St. J. Russell, "Photonic-Crystal Fibers," *J. Light. Technol.* **24**(12), 4729–4749 (2006).
8. C. R. Rosberg, F. H. Bennet, D. N. Neshev, P. D. Rasmussen, O. Bang, W. Krolikowski, A. Bjarklev, and Y. S. Kivshar, "Tunable diffraction and self-defocusing in liquid-filled photonic crystal fibers," *Opt. Express* **15**(19), 12145–12150 (2007).
9. H. W. Lee, M. A. Schmidt, H. K. Tyagi, L. Prill Sempere, and P. St. J. Russell, "Polarization-dependent coupling to plasmon modes on submicron gold wire in photonic crystal fiber," *Appl. Phys. Lett.* **93**(11), 10–13 (2008).
10. A. Lorenz, H.-S. Kitzerow, A. Schwuchow, J. Kobelke, and H. Bartelt, "Photonic crystal fiber with a dual-frequency addressable liquid crystal, behavior in the visible wavelength range," *Opt. Express* **16**(23), 19375–19381 (2008).
11. M. Vieweg, T. Gissibl, S. Pricking, B. T. Kuhlmeier, D. C. Wu, B. J. Eggleton, and H. Giessen, "Ultrafast nonlinear optofluidics in selectively liquid-filled photonic crystal fibers," *Opt. Express* **18**(24), 25232 (2010).
12. M. Wahle and H. Kitzerow, "Measurement of group velocity dispersion in a solid-core photonic crystal fiber filled with a nematic liquid crystal," *Opt. Lett.* **39**(16), 4816–4819 (2014).
13. F. Luan, A. K. George, T. D. Hedley, G. J. Pearce, David M Bird, J. C. Knight, and P. St. J. Russell, "All-solid photonic bandgap fiber," *Opt. Lett.* **29**(20), 2369–2371 (2004).
14. T. A. Birks, G. J. Pearce, and D. M. Bird, "Approximate band structure calculation for photonic bandgap fibres," *Opt. Express* **14**(20), 9483–9490 (2006).
15. A. Argyros, T. A. Birks, S. G. Leon-Saval, C. M. B. Cordeiro, F. Luan, and P. St. J. Russell, "Photonic bandgap with an index step of one percent," *Opt. Express*, **13**(1), 309 (2005).
16. N. Litchinitser, S. Dunn, P. Steinvurzel, B. Eggleton, T. White, R. McPhedran, and C. de Sterke, "Application of an ARROW model for designing tunable photonic devices," *Opt. Express* **12**(8), 1540–50 (2004).

17. T. Larsen, A. Bjarklev, D. Hermann, and J. Broeng, "Optical devices based on liquid crystal photonic bandgap fibres," *Opt. Express* **11**(20), 2589–96, oct 2003.
18. K. Milenko, T. R. Wolinski, P. P. Shum, and D. J. Juan Hu, "Temperature-Sensitive Photonic Liquid Crystal Fiber Modal Interferometer," *IEEE Photonics J.* **4**(5), 1855–1860 (2012).
19. Lara Scolari, Thomas Alkeskjold, Jesper Riishede, Anders Bjarklev, David Hermann, Anawati Anawati, Martin Nielsen, and Paolo Bassi, "Continuously tunable devices based on electrical control of dual-frequency liquid crystal filled photonic bandgap fibers," *Opt. Express* **13**(19), 7483–7496 (2005).
20. Alexander Lorenz, Rolf Schuhmann, and Heinz-Siegfried Kitzerow, "Switchable waveguiding in two liquid-crystal-filled photonic crystal fibers," *Appl. Opt.* **49**(20), 3846–3853 (2010).
21. M. Wahle and H.-S. Kitzerow, "Electrically tunable zero dispersion wavelengths in photonic crystal fibers filled with a dual frequency addressable liquid crystal," *Appl. Phys. Lett.* **107**(20), 201114 (2015).
22. I. C. Khoo, K. L. Hong, S. Zhao, D. Ma, and T.-H. Lin, "Blue-phase liquid crystal cored optical fiber array with photonic bandgaps and nonlinear transmission properties," *Opt. Express* **21**(4), 4319–27 (2013).
23. D. Poudereux, K. Orzechowski, O. Chojnowska, M. Tefelska, T. R. Wolinski, and J. M. Otón, "Infiltration of a photonic crystal fiber with cholesteric liquid crystal and blue phase," *Proc. SPIE* **9290**, 92900 (2014).
24. Y. Chen, D. Xu, S.-t. Wu, S.-i. Yamamoto, and Y. Haseba, "A low voltage and submillisecond-response polymer-stabilized blue phase liquid crystal," *Appl. Phys. Lett.* **102**(14), 141116 (2013).
25. P. R. Gerber, "Electro-Optical Effects of a Small-Pitch Blue-Phase System," *Mol. Cryst. Liq. Cryst.* **116**(3-4), 197–206 (1985).
26. J. Yan, H.-C. Cheng, S. Gauza, Y. Li, M. Jiao, L. Rao, and S. T. Wu, "Extended Kerr effect of polymer-stabilized blue-phase liquid crystals," *Appl. Phys. Lett.* **96**(7), 071105 (2010).
27. N. M. Litchinitser, A. K. Abeeluck, C. Headley, and B. J. Eggleton, "Antiresonant reflecting photonic crystal optical waveguides," *Opt. Lett.* **27**(18), 1592–1594 (2002).
28. P. Steinvurzel, B. T. Kuhlmeiy, T. P. White, M.J. Steel, C. Martijn de Sterke, and B. J. Eggleton, "Long wavelength anti-resonant guidance in high index inclusion microstructured fibers," *Opt. Express* **12**, 5424–5433 (2004).
29. A. W. Snyder and J. D. Love, *Optical Waveguide Theory*, 2nd ed. (Springer, 1983).
30. P. Steinvurzel, C. Martijn de Sterke, M. J. Steel, B. T. Kuhlmeiy, and B. J. Eggleton, "Single scatterer Fano resonances in solid core photonic band gap fibers," *Opt. Express* **14**, 8797–8811 (2006).
31. John David Jackson, *Classical Electrodynamics*, 3rd Ed. (Wiley, 1999).
32. S. M. Sze and K. K. Ng, *Physics of Semiconductor Devices*, 3rd Ed. (John Wiley and Sons, 2006).
33. Comsol 4.2, www.comsol.com.
34. I. H. Malitson, "Interspecimen Comparison of the Refractive Index of Fused Silica," *J. Opt. Soc. Am.* **55**(10), 1205 (1965).
35. G. Ren, P. Shum, J. Hu, X. Yu, and Y. Gong, "Polarization-dependent bandgap splitting and mode guiding in liquid crystal photonic bandgap fibers," *J. Light. Technol.* **26**(22), 3650–3659 (2008).
36. K. Busch and S. John, "Photonic band gap formation in certain self-organizing systems," *Phys. Rev. E* **58**(3), 3896–3908 (1998).
37. R. Spittel, H. Bartelt, and M. Schmidt, "A semi-analytical model for the approximation of plasmonic bands in arrays of metal wires in photonic crystal fibers," *Opt. Express* **22**(10), 11741 (2014).

1. Introduction

Blue phases (BPs) are chiral liquid crystalline phases which exhibit a three dimensional structure. The lattice constant of this structure is commonly in the range of the wavelengths of visible light. This leads to brilliantly reflecting domains seen in a polarizing microscope [Fig. 1(a)]. Three different blue phase modifications can appear in the absence of external fields, but only two of them, BP I and II, show a periodic structure [1]. For the BP I and BP II, the three dimensional structure is composed of double twist cylinders [Fig. 1(b)] stacked in a cubic lattice [1, 2]. This cubic super structure makes BPs optically isotropic in the absence of external electric or magnetic fields.

Under the influence of an external electric field, the BP becomes birefringent with its optical axis oriented along the direction of the electric field. This is usually a fast process ($\lesssim 1$ ms [3–6]) compared to nematic liquid crystals (~ 10 ms). Thus, BPs are of current interest in display research. Another advantage is that BPs do not require surface alignment for a homogeneous orientation. This gives them an advantage over other liquid crystalline phases, which usually require high quality alignment layers. As there is no need for this additional layer, blue phases are excellent candidates for use in confined geometries like photonic crystal fibers (PCFs).

PCFs are optical fibers which confine light by a periodic array of air inclusions [7] in a glass

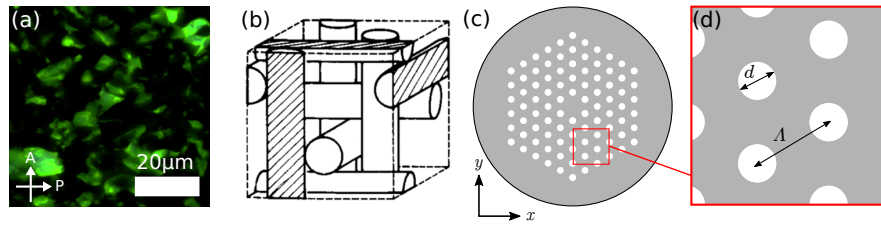


Fig. 1. (a) Polarizing optical microscope image of a blue phase I in reflection. (b) Cubic arrangement of double twist cylinders in a blue phase I unit cell [6]. (c) Schematic of the cross section of a photonic crystal fibers. (d) Close-up of the period cladding with inclusion diameter d and pitch Λ .

matrix [Fig. 1(c) and (d)]. The light guiding core is formed by one or more missing inclusions. The air inclusions can be easily filled with various liquids by capillary action [8–12]. If the refractive index of the liquid is higher than the index of the surrounding material, light guidance is supported by photonic band gaps (PBGs) of the cladding [13–15]. The PBGs reflect the light impinging on the walls and confine it to the core. But there are wavelength regions, where light is not confined because a single PBG only covers a certain wavelength range. Thus, the transmission spectrum of such a fiber exhibits multiple regions of low transmission. These regions are referred to as photonic bands, which exist inside the cladding.

The positions of the photonic bands (and photonic band gaps) are determined by the refractive index of the inclusions and the surrounding materials [16]. Thus liquid crystals have been commonly used to control the optical transmission through these fibers. The refractive indices of the LCs can be influenced via temperature change [17, 18] or electromagnetic fields [19–21].

Choosing blue phases instead of nematic liquid crystals to infiltrate PCFs provides some advantages. There is no need for an alignment, layer which simplifies the experiment. Further, the theoretical description is simplified as BPs are isotropic in the field off-state. Thus, complicated liquid crystal director fields have not to be taken into account.

So far, only thermal tuning of blue phase photonic crystal fibers (BPPCFs) has been investigated [22, 23] in order to change the transmission. This is generally a slow process. From our point of view, the tuning via electrical fields is a more promising concept. This option has become viable only recently, when blue phases with high sensitivity to electric fields (high Kerr constants) have become available [4, 5, 24].

In this article, we discuss the effect of electrically induced uniaxiality of the blue phase on the polarization dependent transmission of BPPCFs. We interpret the experimental results with the help of modal analysis and band gap analysis via the finite element method. Finally, we connect the changes in the band gap guidance to the Kerr constant of the blue phase material.

2. Background

2.1. Blue phases

The cubic arrangement of double twist cylinders [Fig. 1(b)] leads to a macroscopically isotropic liquid crystalline blue phase with the refractive index n_{BP} . An external electric field induces a threshold-less reorientation of molecules; the BP becomes birefringent. The blue phase then resembles a uniaxial medium. Its optical axis is oriented along direction of the external electric field as shown in Fig. 2(a). For small electric field strengths, field-induced biaxiality and saturation can be neglected. If so, the birefringence δn can be modeled by the Kerr effect of an initially isotropic medium [25, 26]

$$\delta n = K \lambda E^2, \quad (1)$$

where K is the Kerr constant, λ the wavelength of the light and E the electric field. The refractive indices parallel (n_e) and perpendicular (n_o) to the optical axis can be expressed by

$$n_o = n_{BP} - \frac{1}{3} \delta n \quad \text{and} \quad n_e = n_{BP} + \frac{2}{3} \delta n, \quad (2)$$

where δn is the field-induced birefringence. For very large electric field strengths, the chiral structure becomes unwound to a nematic state. δn then approaches a saturation value $\Delta n(T)$, which corresponds approximately to the birefringence of the nematic phase that appears in a racemic mixture instead of a BP.

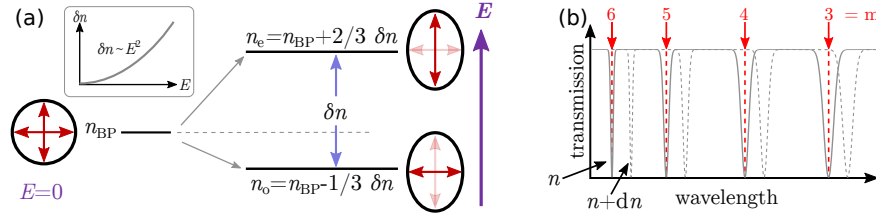


Fig. 2. (a) Splitting of the refractive index of the initially isotropic blue phase due to an electric field. The blue phase becomes uniaxial with ordinary refractive index n_o and extraordinary refractive index n_e . The inset shows the quadratic dependence of the induced birefringence δn on the electric field. (b) Schematic of the transmission (solid line) through an ARROW structure, in which the inclusion material has an isotropic refractive index n . The resonances are labeled according to the corresponding order m and are marked with red lines. The dashed gray line shows the transmission if the refractive index is increased by $dn > 0$. The change dn is isotropic.

2.2. Photonic crystal fibers

The periodic arrangement of air holes in photonic crystal fibers can be filled with a high index material. ‘High’ means that the refractive index of the material is larger than the refractive index of the background material. Then the light is confined by photonic band gaps. These fibers are therefore also referred to as photonic band gap fibers. However, the cladding does not provide a full band gap over a broad spectral range but is interrupted by photonic bands. Within these photonic bands the light escapes from the core into the cladding and a spectral region of low transmission arises.

A closer inspection of these photonic bands reveals that they closely resemble waveguide modes of the individual inclusions [14]. The regions of low transmission can then be interpreted as wavelengths where the core mode is in resonance with the photonic bands. Then, strong coupling occurs and light is distributed over the cladding. Consequently, light is only guided if the core modes and the photonic bands are anti-resonant. This interpretation is called the anti-resonant reflecting optical waveguide (ARROW) model [16, 27, 28].

According to this model, a strong interaction between the core mode and a photonic band is expected only close to the cutoff of the involved inclusion mode. The cutoff conditions for the inclusion modes are well known [29]. The positions can be approximated by [16, 30]

$$\lambda_m = \frac{4d}{2m + 1} (n^2 - n_s^2)^{1/2}, \quad (3)$$

where λ_m is the m -th expected ARROW resonance wavelength, d is the inclusion diameter, n is the refractive index of the inclusion and n_s is the refractive index of the surrounding material. Figure 2(b) shows schematically a transmission spectrum of an ARROW fiber. The positions of the dips in transmission can be predicted and labeled with Eq. (3).

2.3. Blue phase photonic crystal fibers

Equation (3) gives a relation between the transmission minima in a BPPCF and the refractive index of the inclusions. If we consider the blue phase to be the high index material, we can calculate the refractive index from the transmission dips.

If an electric field is applied along the fiber cross section, the refractive index of the blue phase changes from n_{BP} to \tilde{n}_{BP} for a specific direction. From Eq. (3) it is clear that then λ_m shifts to $\tilde{\lambda}_m$. The shift in wavelength can be measured. In order to get a relation between the shift in wavelength and the change in refractive index, we use $\tilde{n}_{BP} = n_{BP} + dn$ and assume that $dn \ll 1$. The latter condition is reasonable as we work with low electric fields. Then we can approximate the square of the refractive index in Eq. (3) by $\tilde{n}_{BP}^2 \approx n_{BP}^2 + 2n_{BP}dn$. Equation (3) can then be rearranged to

$$dn \approx \left(\frac{2m+1}{4d} \right)^2 \frac{1}{2n_{BP}} (\tilde{\lambda}_m^2 - \lambda_m^2)^{1/2}. \quad (4)$$

This equation relates the shift in wavelength of a band to the corresponding change in refractive index.

3. Materials and setup

For the experiments, a commercial PCF (LMA10, NKT photonics) made of silica with inclusion diameter $d = 2.908 \mu\text{m}$, pitch $\Lambda = 6.525 \mu\text{m}$ [cf. Fig. 1(d)] and outer diameter $D = 125 \mu\text{m}$ is filled with the blue phase mixture by capillary forces. This mixture consists of 97.2% liquid crystal host MDA-PB-3 [5] provided by Merck doped with 2.8% of the chiral component R5011.

The permittivities of the neat MDA-PB-3 have been measured at different temperatures at 1 kHz. At 68°C , which is close to the blue phase temperature region of the prepared mixture, the values for the permittivities are $\epsilon_{\perp} = 13$, $\epsilon_{\parallel} = 55$ and $\bar{\epsilon} = \frac{2}{3}\epsilon_{\perp} + \frac{1}{3}\epsilon_{\parallel} = 27$. We assume that the blue phase permittivity ϵ_{BP} is approximately equal to the average permittivity, i. e. $\epsilon_{BP} \approx \bar{\epsilon}$. The refractive indices at room temperature for the neat MDA-PB-3 are $n_o = 1.489$ for the ordinary index and $n_e = 1.664$ for the extraordinary index (measured with an Abbe refractometer at 589 nm). The refractive index of the blue phase can be found in the inset of Fig. 7.

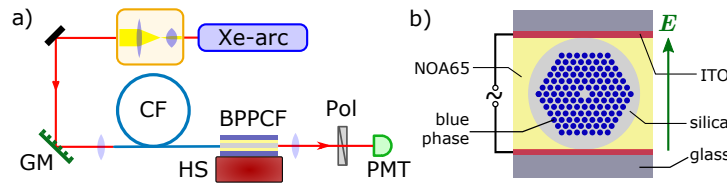


Fig. 3. (a) Setup for measuring the transmission through a blue phase photonic crystal fiber. The light of a broad band Xe-arc lamp is collimated, then passes through a grating monochromator (GM). The monochromatic light is coupled into a fiber (CF) which is butt-coupled to the BPPCF and placed on a hot stage (HS). The transmitted light passes through a polarizer (Pol) and is detected by a photo multiplier tube (PMT). (b) The BPPCF sample is sandwiched between conducting ITO plates and fixed with an adhesive NOA65 (Norland Optical Adhesive 65).

The transmission of the sample is measured with the setup shown in Fig. 3(a). All measurements are performed upon heating. The BPPCF of 3.3 cm length is fixed between conducting ITO plates [Fig. 3(b)] to apply an external voltage V . The electric field inside the inclusions E_{incl} can be approximated by

$$E_{\text{incl}} = \frac{2\epsilon_s}{\epsilon_{BP} + \epsilon_s} \frac{V}{D} \quad (5)$$

where D is the distance between the conduction plates, which is identical with the fiber diameter, ϵ_s and ϵ_{BP} are the relative permittivities of the surrounding medium (silica) and the blue phase, respectively. Details about this equation can be found in the Appendix A.

4. Results and discussion

4.1. Measuring the transmission under the influence of an electric field

After filling the BP into the PCF, polarizing microscope images of the fiber were studied upon heating [Fig. 4]. The transition from the cholesteric phase (a) to BP I (b,c) to BP II (d,e) and then the BP II-isotropic coexistence (f) is observed between 65.5 °C and 67.5 °C. Within the blue phase regions, indeed blue phase platelets are observed. For BP I, also different orientations of the BP crystals can be observed.

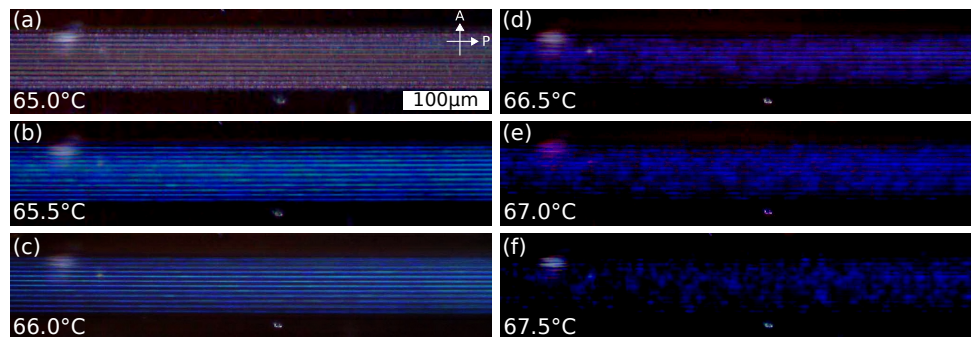


Fig. 4. Polarizing microscope images of a BPPCF in transmission for different temperatures: (a) the cholesteric phase, (b, c) BP I, (d, e) BP II and (f) BP II-isotropic coexistence.

Figure 5(a) and (b) show the results of the transmission measurements in the visible wavelength range for voltages from 0 V to 600 V. The polarization of the light is (a) perpendicular (x -polarized) and (b) parallel (y -polarized) to the external electric field [cf. Fig. 3(b)]. At 0 V, the spectra show transmission windows which are expected for a photonic band gap fiber. The spectra for x - and y -polarization at 0 V confirm that the blue phase is isotropic as both spectra are almost identical.

Under application of a square wave at 1 kHz, the average intensity in the case of x -polarization [Fig. 5(a)] decreases by 23 % at 600 V. This loss of intensity can be attributed to scattering by the change in refractive index when the electric field switches polarity. The loss increases with increasing voltage, i. e. with increasing induced birefringence. The position of the band gaps, however, is not affected in any way.

In the case of y polarized light [Fig. 5(b)], a much stronger decrease in intensity with increasing voltage (45 % at 600 V) is observed. The scattering in this case is higher because it relates to the birefringence which is larger for the y -polarization [$+2/3 \delta n$, cf. Eq. (2)] than for the x -polarization [$-1/3 \delta n$]. In contrast to the x -polarized light, the y -polarized light also shows a shift of the band gap positions, the magnitude of which increases with the voltage. To make this effect more visible we focus on a single band gap [gray shaded in Fig. 5(a) and 5(b)].

In Fig. 5(c) and 5(d) the band gap located between 530 nm and 620 nm is plotted for (c) x - and (d) y -polarized light. The intensities are normalized to unity for each voltage in both graphs. This procedure reveals that there is almost no change of the band gap shape for the x -polarized case. In contrast, for y -polarized light, there is a significant shift of the left edge of the transmission window by up to 12 nm at 600 V while the right edge remains constant. This effect of an asymmetric shift of the transmission windows will be discussed in the following section.

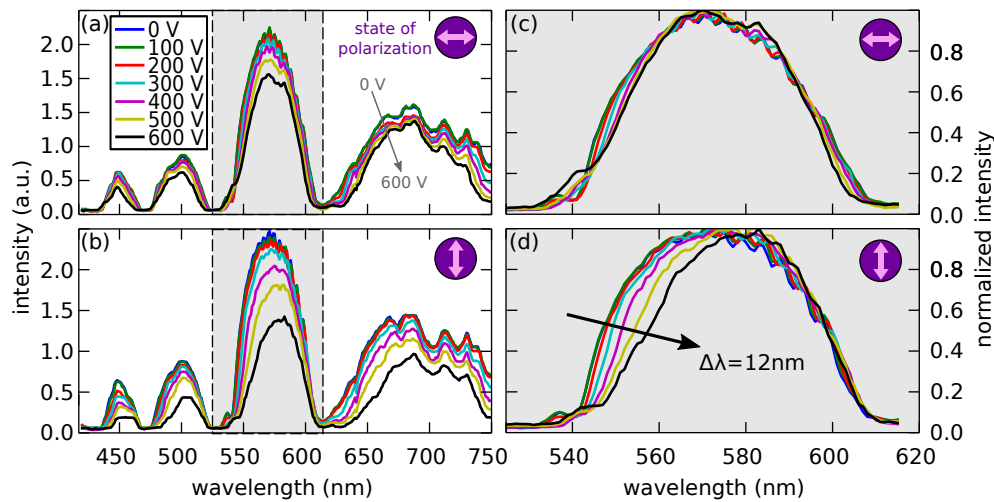


Fig. 5. Transmission spectra of white light coupled into a BPPCF for different voltages. (a) Polarization of light (x direction) is perpendicular to the external electric field, (b) polarization is parallel to the electric field. (c) and (d) are enlargements of (a) and (b) for the band gap around 575 nm. The spectra are recorded at 65.5 °C.

4.2. Explaining the asymmetric shift

From the ARROW model and Eq. (4), a symmetric shift of the band gap is expected. To investigate this behavior, we carried out a modal analysis via the finite element method (FEM). In Fig. 6(a) the fraction of the electric field guided in the core is plotted for three different cases: (i) in the absence of an electric field (blue line) meaning at 0 V where the blue phase is isotropic; (ii) with an applied voltage of 650 V taking into account the correct anisotropy with $n_x = n_z = n_o$, $n_y = n_e$ (green line) and (iii) also at 650 V but with an ‘artificial’ refractive index distribution $n_x = n_y = n_e$, $n_z = n_o$ (red line). The last case is an anisotropic waveguide with its optical axis parallel to the fiber axis. The cases (i) and (ii) represent the experiment at 0 V and 650 V, respectively.

The simulation in fact shows a shift of the short wavelength edge of the transmission window from case (i) to (ii). On the long wavelength edge in case (ii), the core power drops to 0.2 at 610 nm which coincides with edge of the transmission window in case (i). In the range from 610 nm to 615 nm the core power stays low indicating weak confinement of the core mode. This is the region we do not see in the experiment due to the high losses. Beyond 615 nm the core mode is not confined anymore. In case (iii), the wavelength region between 610 nm and 615 nm exhibits good confinement of the core mode. Thus, we conclude that the asymmetric shift originates from the anisotropy when the optical axis is perpendicular to the fiber axis.

This result is supported by the modal analysis [Fig. 6(b)] at 610 nm. It reveals that the mode in case (ii) couples to a photonic band (or cladding mode) which is mainly x -polarized. The coupling is weak because the core mode is y -polarized. The photonic band does not move to longer wavelengths under voltage as its polarization is mainly perpendicular to the polarization direction with increasing refractive index. In case (iii), this photonic band is not present because it has shifted to longer wavelengths due to $n_e = n_x = n_y$.

The above interpretation is supported by the band gap plots in Fig. 6(c) and 6(d). Details on the simulations are given in Appendix B. Fig. 6(c) shows the band gap diagram at 0 V [case (i)]. The effective refractive index of the guided mode is shown in green and has been obtained by modal analysis. It is flanked by two photonic bands located around 537 nm and 612 nm. The

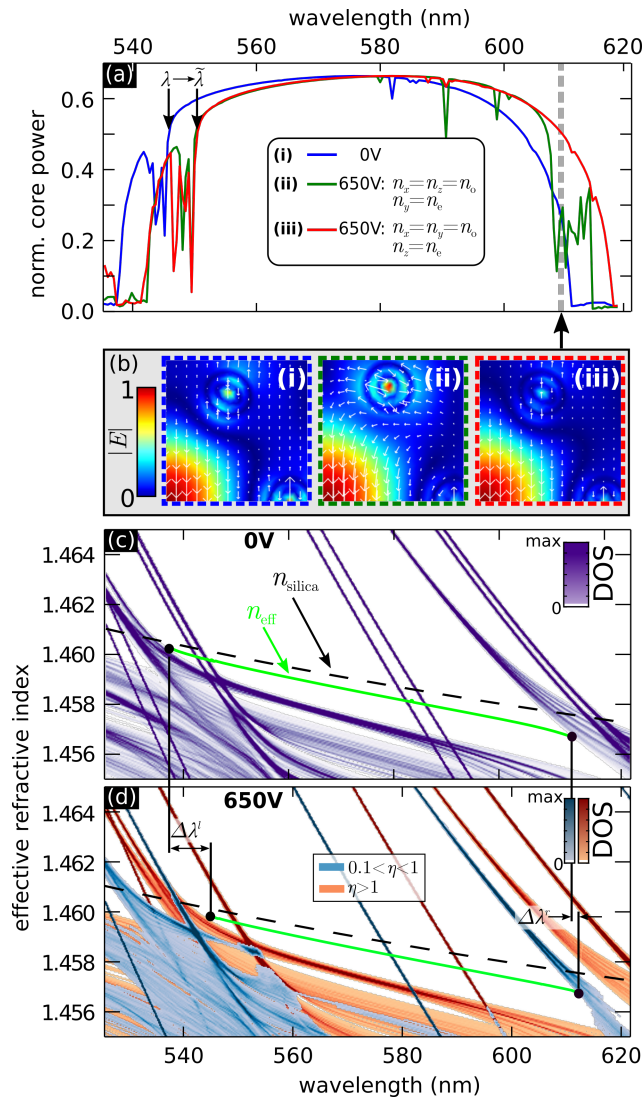


Fig. 6. (a) Electric field confined to the core of the fundamental mode of a single band gap around 580 nm for three different cases (i) 0 V (blue), (ii) 650 V with $n_y = n_e, n_x = n_z = n_o$ (green) and (iii) $n_y = n_x = n_e, n_z = n_o$ (red). On the short wavelength edge, we marked the wavelength shift $\lambda \rightarrow \tilde{\lambda}$. (b) Simulated mode profiles (normalized electric field) at 610 nm for the described cases. Each image is $7 \mu\text{m} \times 7 \mu\text{m}$. (c) DOS plot for 0 V (case (i)). (d) DOS plot for 650 V (case (ii)): the orange regions correspond to bands with $\eta \leq 1$ and the blue regions to bands with $0.1 \leq \eta < 1$. The green line in (c) and (d) corresponds to the effective refractive index of the guided mode. The wavelength shift of the band edges ($\Delta\lambda^l$ and $\Delta\lambda^r$) of the transmission window are marked separately for short and long wavelength edge. For the simulation, $K = 6.0 \text{ nm V}^{-2}$ is assumed.

interaction of the core mode with the photonic bands leads to a bending of the effective refractive index close to the edges. There are some bands (at 548 nm and 585 nm) within the transmission window which intersect with the core mode but do not interact. These are caused by higher order cladding modes, the high order of which does not allow for significant coupling [16].

At a voltage of 650 V [case (ii), Fig. 6(d)], the bands start to shift and polarization dependencies

of the photonic bands start to appear. To distinguish between the polarizations of the bands we introduce a parameter $\eta = \langle |E_y| \rangle / \langle |E_x| \rangle$, where $\langle |E_x| \rangle$ and $\langle |E_y| \rangle$ are the absolute values of electric fields E_x and E_y averaged for a photonic band. The plot now shows two different kinds of photonic bands. Bands with $\eta > 1$ [orange in Fig. 6(d)] are mainly y -polarized and bands with $0.1 < \eta < 1$ (blue) are predominantly x -polarized but still carry some amount of y -polarization.

The region in which the core mode (green line) is guided becomes smaller with increasing voltage. On the short wavelength side, a mainly y -polarized band ($\eta > 1$) flanks the core mode at 543 nm. In contrast, the core mode is stopped on the long wavelength edge at 615 nm by a band which is predominantly x -polarized (blue). The left band is shifted significantly due to its strong response to the increase of the refractive index n_y . The right edge approximately stays constant because it is mostly x -polarized and interacts with n_x . This leads to the asymmetric shift of the transmission window.

4.3. Applying the ARROW model to determine the Kerr constant

From the previous discussion it is clear that the induced change in refractive index of the blue phase causes the left edges of the transmission windows to shift. We now want to connect the applied electric field to the shift in wavelength and then to the induced birefringence. Finally, we would like to evaluate if the birefringence is proportional to the electric field squared as described by Eq. (1).

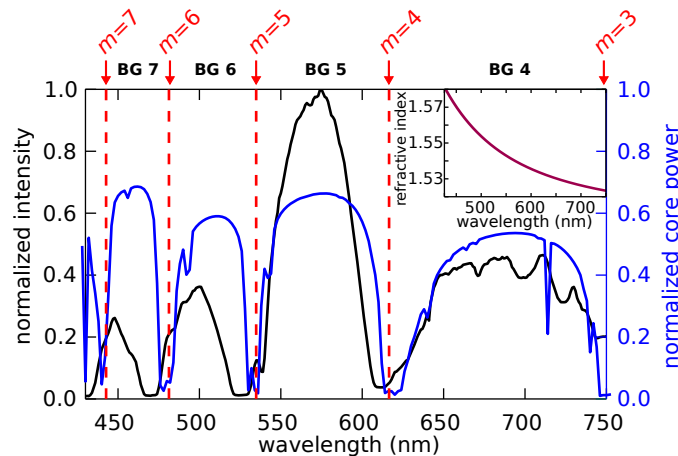


Fig. 7. The solid black line corresponds to the measured intensity and the cyan line shows the simulated power confined to the core. The red labels on the top give the respective m -values determined by the ARROW model. The band gaps are labeled correspondingly. The inset shows the refractive index of the blue phase material at 0 V and 68 °C.

Equation (4) gives us a relation between the shift of the photonic band and the corresponding change in refractive index. This equation is based on the ARROW model and we require the band or resonance order m to use Eq. (4). To this end, we plot in Fig. 7 the measured transmission spectrum and the transmission dips predicted by the ARROW model. The results show good agreement between the ARROW model and the experiment. There are some differences towards the shorter wavelengths, though. These differences are due to the inaccuracy of the measured refractive index of the blue phase n_{BP} . To verify this, we plotted the normalized power guided inside the core region. This is in perfect agreement with the ARROW model and in good agreement with the experiment. The numbering of the photonic bands (or resonances) can then be performed: $m = 3, \dots, 7$ from right to left.

Now that we have identified the resonance order m for the corresponding band gaps, we determine the electrically induced wavelength shift $\tilde{\lambda}_m$ of the short wavelength edges in Fig. 5(b). For each band gap and each voltage $\tilde{\lambda}_m$ are analyzed at five positions of the normalized intensity ($I = 0.3, 0.4, \dots, 0.7$).

The change in refractive index is then obtained with Eq. (4). If we then assume that the shift in wavelength and therefore the change in refractive index is solely caused by the extraordinary refractive index n_e , i. e. $dn = n_e - n_{BP}$, we are able to relate dn to the induced birefringence in Eq. (1) by $\delta n = 3/2dn$.

From Eq. (1) it is expected that δn is linear with the electric field squared. Therefore, in Fig. 8(a) we plot δn against E^2 for each photonic band at temperature $T = 65.5^\circ\text{C}$. All photonic bands show the expected linear behavior. For the bands $m = 5$ and $m = 6$, the agreement is very good. For the bands $m = 4$ and $m = 7$, the deviations are quite high. The Kerr constant K is calculated from the slope of the linear fit. The Kerr constants vary with band number from 5.53 nm V^{-2} for $m = 4$ to 7.01 nm V^{-2} for $m = 5$.

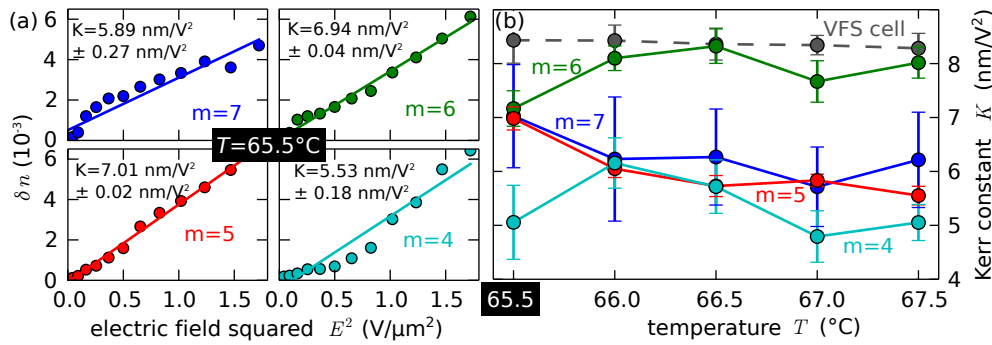


Fig. 8. (a) Electrically induced birefringence δn (filled circles) calculated with the ARROW model for the each band gap at 65.5°C . The Kerr constant is calculated from the linear fit (solid line). (b) Kerr constants of the different photonic bands versus temperature. The gray dashed line shows the Kerr constant that we measured in a vertical field switching (VFS) cell.

The Kerr constants also change with temperature as can be seen in Fig. 8(b). In general Kerr constants seem to decrease, which is commonly observed in blue phases. The band with $m = 6$ is distinct from the remaining bands by its high Kerr constant of about 8 nm V^{-2} . This value comes close to the values of the Kerr constant measured in a vertical field switching (VFS) cell (dashed grey line). At all temperatures, the Kerr constants of all photonic bands are lower than the ones measured in the VFS cell. This is again an effect of the bands carrying a mixed polarization. Even though they are mainly influenced by the y -component of the refractive index ($n_y = n_e$), they still weakly interact with the lower index $n_x = n_o$. Each photonic band carries different portions of x and y -polarizations and hence shows different Kerr constants.

These results seem to limit the applicability of the ARROW model, which is made for isotropic materials. Nevertheless, there still is a linear relation between the shift of the photonic bands and the electric field squared as it is predicted by Eqs. 1 and 4. The refractive index change we calculated above has to be seen as an effective value and consequently the Kerr constant has to be seen this way. The merit of these values is that with them we are able to predict how the left edge of a specific transmission window shifts for a given electric field.

5. Conclusion

In this work, we infiltrated a photonic crystal fiber with a liquid crystalline blue phase and electrically induced a birefringence of the blue phase with an optical axis perpendicular to the

fiber axis. Consequently, the transmission spectrum of the fiber became strongly polarization dependent. For the polarization of light perpendicular to the optical axis, almost no change in transmission windows was found. However, the transmission windows for light polarized parallel to the optical axis shifted to longer wavelengths. In the latter case, the change was strongly asymmetric. While the long wavelength edge remained constant, the short wavelength edge shifted proportional to the square of the electric field.

By band gap analysis of the photonic cladding, we found that the photonic bands of the short wavelength edge were mainly polarized along the optical axis. The increased refractive index had therefore strong effect on these bands, which led to a red-shift. However, the long wavelength edge was formed by bands mainly polarized perpendicular to the optical axis. They did therefore not shift. Nevertheless, these photonic bands still carried sufficient polarization to stop the core mode.

We then used the shift of the short wavelength edge to determine the change in refractive index. We discovered that the induced shift is indeed proportional to the electric field squared as expected of a Kerr medium. From this, we calculated the Kerr constants, which are lower than the Kerr constant measured in the bulk material. This can be attributed to the mixed polarization of the photonic bands.

Blue phases offer the unique opportunity to study a uniaxial medium within a photonic crystal fiber where the optical axis is distinct from the fiber axis. This provides a new application for the electrooptic effects observed in blue phases.

Appendix A: Electric field inside inclusions

Equation (5) describes the electric field inside the inclusion. This field is different from the electric field within the surrounding material due to the difference in permittivity [31]. The field can be approximated by the limit of a single inclusion which is embedded in the middle of an otherwise perfect plate capacitor. This is possible because the relative permittivities of silica [32] and the optical adhesive are very similar (≈ 3.9). Then, by performing a multipole expansion [31], it can be shown that the external field $E_{\text{ex}} = V/D$ and the inclusion field are related by Eq. (5). For the given parameters this results in $E_{\text{incl}} \approx 0.25E_{\text{ex}}$. It is important to note, that within this approximation the field inside the inclusion is homogeneous. However, as there are not one but multiple inclusions close to each other inside the silica surrounding, there will be deviations both inside a specific inclusion and also when comparing different inclusions. The variations can be up to 15%. The variations are not considered in the calculations of photonic band or the Kerr constant.

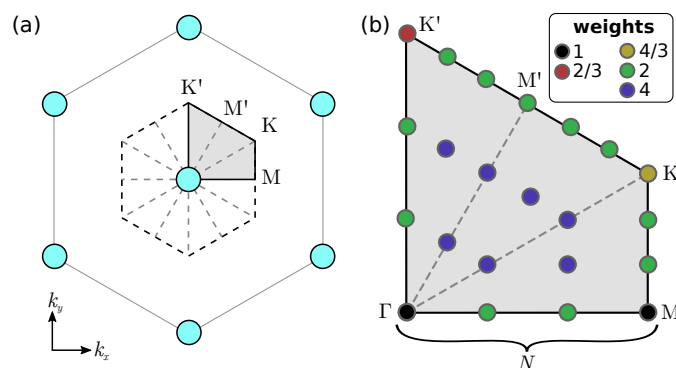


Fig. 9. (a) Unit cell of the hexagonal photonic crystal cladding in k -space. (b) A quarter of the first Brillouin zone for an uniaxial lattice with optical axis along the y direction. The points represent the discretization of the k -vectors for N nodes per edge. The different node colors indicate the weighting of the node due to symmetry arguments.

Appendix B: Band gap simulations

The calculations of the photonic band gaps in Fig. 6(c) and 6(d) were carried out with the finite element software COMSOL Multiphysics [33]. The dispersion of silica [34] and the blue phase [cf. inset in Fig. 7] have been taken into account. Due to the anisotropy of the blue phase material under voltage, it is necessary to simulate a quarter of the hexagonal unit cell [35] instead of one twelfth in the isotropic case [Fig. 9(a)]. Fig. 9(b) shows the reduced unit cell. The discretization of the k -vectors is characterized by N nodes per edge leading to $(3N - 1)N/2$ in total. For the simulations we used $N = 7$ corresponding to overall 70 points in k -space. Each node has to be weighted [36, 37] to compensate for overcounting of certain nodes. The weighting is indicated in Fig. 9(b).

Funding

German Research Foundation (DFG) graduate school GRK1464. The support by the DFG is gratefully acknowledged.